Defect characterization of InAs/InGaAs quantum dot p-i-n photodetector grown on GaAs-on-V-grooved-Si substrate

Jian Huang, [†, ‡] Yating Wan, [‖, ‡] Daehwan Jung, [‖, §] Justin Norman, [⊥] Chen Shang, [⊥] Qiang Li, [#] Kei May Lau, [#] Arthur C. Gossard, [‖, ⊥] John E. Bowers, [‖, ⊥] and Baile Chen [†, *]

[†] Optoelectronic Device Laboratory, School of Information Science and Technology, ShanghaiTech University, Shanghai 201210, China

[‖] Institute for Energy Efficiency, University of California Santa Barbara, Santa Barbara, California 93106, USA

[§] Center for Opto-Electronics Materials and Devices, Korea Institute of Science and Technology, Seoul, 02792, South Korea

[⊥] Materials Department, University of California Santa Barbara, Santa Barbara, California 93106, USA

[#] Department of Electronic and Computer Engineering, Hong Kong University of Science & Technology, Clear Water Bay, Hong Kong

KEYWORDS: quantum dots, silicon, photodetector, low frequency noise, defect analysis

ABSTRACT: The performance of semiconductor devices on silicon can be severely degraded by the presence of dislocations incurred during heteroepitaxial growth. Here, the physics of the defect mechanisms, characterization of epitaxial structures and device properties of waveguide photodetectors (PDs) epitaxially grown on (001) Si is presented. A special GaAs-on-V-grooved-Si template was prepared by combining the aspect ratio trapping effects, superlattice cyclic, and strain-balancing layer stacks. A high quality of buffer structure was characterized by atomic force microscopy (AFM) and electron channeling contrast imaging (ECCI) results. An ultra-low dark current density of 3.5×10^{-7}A/cm^2 at 300 K was measured under -1 V. That is 40 times smaller than the best reported value of epitaxially grown InAs/GaAs quantum dot photodetector structure on GaP/Si substrate. Low frequency noise spectroscopy was used to characterize the generation and recombination related deep levels. A trap with an activation energy of 0.4 eV was identified, which is near the middle bandgap. With low frequency noise spectroscopy along with the current-voltage and capacitance-voltage characterizations, the recombination lifetime of 27 μs and trap density of 5.4×10^{12} cm^{-3} were estimated.

Optoelectronic devices based on semiconductor quantum dots (QDs) have attracted much attention due to the unique physical properties of the zero-dimensional carrier confined system and have been widely applied in photodetectors and lasers [1-6]. Recently, monolithic integration of III-V QDs on Si substrate has gained extensive interests due to its potential to overcome the lack of laser source in silicon photonics [7]. However, the device performance is often limited by the defects caused by the large lattice mismatch between III-V compounds and Si substrate. A concern is that the defects in devices may grow during the operation due to recombination enhanced defect reactions (REDR), which leads to device failure and reliability issues [8-11]. The defects in the III-V QDs on Si structures are often only analyzed by transmission electron microscopy (TEM) visually[12], whereas the detailed information about the associated trap level state has not been investigated. In order to improve the performance of QD based devices, an in-depth characterization and analysis of these defects are crucial.

In this paper, leveraging the selective aspect ratio trapping concept, we produce ultra-low defect density GaAs thin films on exact (001) silicon by direct epitaxy. The substrate with p-i-n epitaxial layers was processed into a waveguide photodetector (PD) structure and low frequency noise spectroscopy (LFNS) characterizations were carried out to identify and quantify the deep level within the PD device for the first time. With the combined effects of ten periods of $In_{0.15}Ga_{0.85}As$/GaAs (5/5 nm) superlattice cyclic and 200 nm $In_{0.15}Ga_{0.85}As$ strain-balancing layer stacks, the threading dislocation density (TDD) of the GaAs-on-V-grooved-Si (GoVS) has been reduced to 5.8×10^6 cm^{-2} in the PD active layers. This translates to a very low dark current of 5.3 pA under -1 V at 300 K, with a good optical responsivity extended out to 1360 nm. The dark current exhibited in the PD is much lower than the previously demonstrated InAs/GaAs QD PD structures grown on Si substrates and is, to the best of our knowledge, the lowest dark-current PD with any kind of absorption type (Ge, InGaAs, etc) on silicon. Based on the LFNS characterization, a trap with activation energy of 0.4 eV is identified, which has a capture cross section of 1.5×10^{-16} cm^2. A simple electrical method along with the information extracted from LFNS was developed to estimate the recombination lifetime and trap density. Carrier lifetime and trap density were calculated to be around 27 μs and 5.4×10^{12} cm^{-3} respectively in the device at 300 K. The defect information found in this work could be useful to

benchmark the III-V quantum dots devices grown on Si substrate.

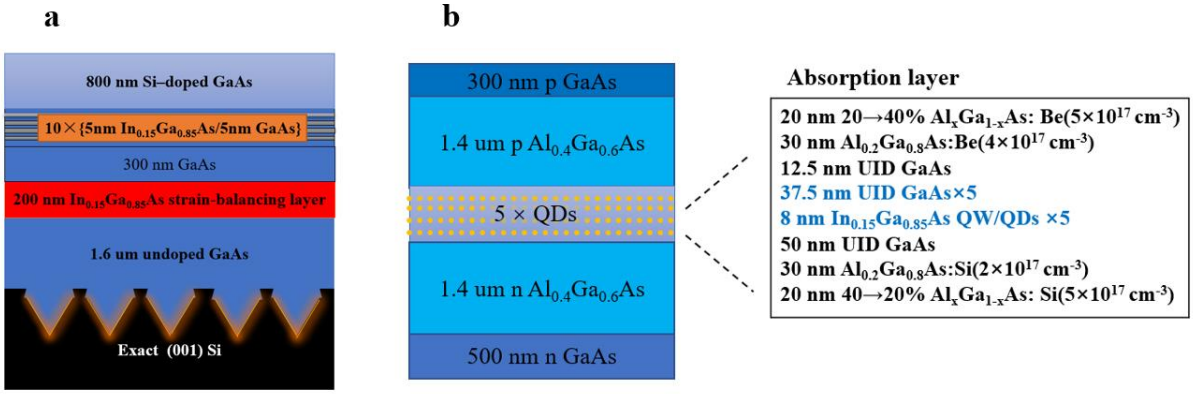

Figure 1. (a) Schematic of the GoVS template. (b) Schematic of the p-i-n PD epitaxial structure grown on GoVS template.

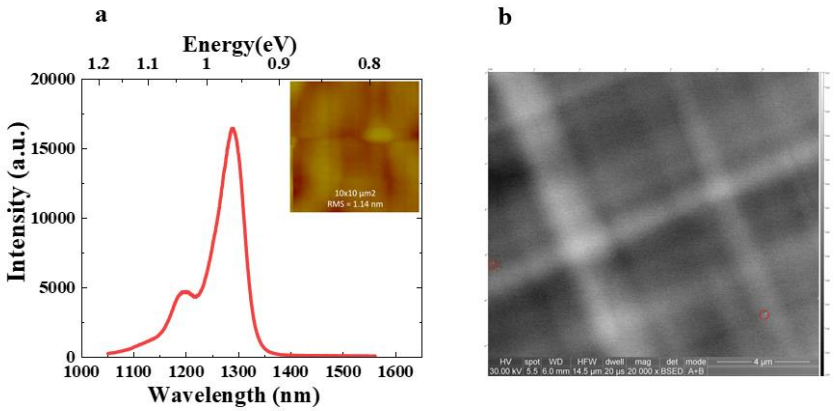

Figure 2. (a) Room temperature PL spectrum of the QDs grown on the GoVS template. Inset: AFM image of the GoVS template, the vertical bar is 10 nm. (b) ECCI of the GoVS template.

RESULTS AND DISCUSSION

Figure 1 shows the schematic of the QD PD structure grown on a GoVS substrate. The GaAs-on-Si substrate was prepared using a V-groove patterned Si substrate by aspect ratio trapping (ART) in a metal-organic chemical vapor deposition (MOCVD) system [13] as shown in Figure 1(a). Ten periods of $In_{0.15}Ga_{0.85}As$/GaAs (5/5 nm) superlattice cyclic and 200 nm $In_{0.15}Ga_{0.85}As$ strain-balancing layer stacks were inserted into the hetero-epitaxial GaAs layer for defects reduction. An p-i-n PD epitaxial structure was grown by molecular beam epitaxy(MBE) system [14] as shown in Figure 1(b). The active region of the PD consists of five-stacked InAs dot-in-a-well (DWELL) structures, with a dot density of 6×10^{10} cm^{-2} [15].

The morphology of GoVS was examined by AFM, as shown in the inset in Figure 2(a). A root mean square (RMS) roughness of 1.14 nm is obtained in a 10×10 μm^2 scanned area which indicates a smooth surface of the GoVS. Electron channeling contrast imaging (ECCI) was used to estimate the threading dislocation density (TDD) of GoVS. A record TDD value of 5.8×10^6 cm^{-2} has been obtained from Figure 2(b). This is a reduction of two orders of magnitude compared with the previous QDs structure grown on silicon template [16].

Room temperature photoluminescence (PL) of the InAs/InGaAs QDs grown on GoVS substrate was conducted by using the 671 nm line from an all-solid-state red laser as the excitation source. In Figure 2(a), the ground-state emission of the QDs grown on the GoVS substrate is at 1288 nm (0.96 eV), with a narrow full-width-at-half maximum (FWHM) of 38 meV. The narrow PL linewidth indicates good size-uniformity of the QDs. At the shorter wavelength, a second peak can be identified, which corresponds to the emission from the excited electron state.

After the material growth, the epitaxial structure was processed into PD devices. A set of rectangular shape mesa waveguides were formed by inductive coupled plasma (ICP) etching. The etched surface was passivated used atomic-layer deposited (ALD) Al_2O_3 together with sputtered SiO_2 layer to help suppress the surface leakage current. The detail fabrication steps can be found in Ref [15]. The inset in Figure 3(b) shows the top-view SEM image of a fabricated device.

Dark current-bias voltage (*I-V*) characteristic of photodetector with width of 30 μm (W) and length of 50 μm length (L) was measured from 150–345 K in a variable temperature probe station with cold shield covered. Data were recorded by a semiconductor device analyzer and were presented in Figure 3(a). For measurements below 270 K, the fluctuations of the PD current are due to the noise limit of

the semiconductor device analyzer. An ultra-low dark current of 5.3×10^{-12}A is obtained under the bias voltage of -1 V at 300K, which corresponds to a dark current density of 3.5×10^{-7}A/cm^2. It is noted that this dark current density is more than 200 times lower than the previous result on GaAs-on-V-grooved-Si template [15] and 40 times lower than the result on GaP/Si substrate [17]. The dark current increases to 1.7×10^{-10}A as the temperature rises to 345 K (corresponding to a dark current density of 1.1×10^{-5}A/cm^2). According to the temperature dependent dark current, the Arrhenius plot is shown in Figure 3(b). An activation energy (E_a) of 0.71 eV is extracted at -0.3 V. This value is about 75% of the bandgap E_g (~0.92 eV) at room temperature. Therefore, the dark current is dominated by both diffusion and generation-recombination (G-R) components [18]. The calculated E_a under different reverse bias was shown in Figure 3(c). The increase of reverse bias extends the depletion region thickness. This contributes to the increase of the G-R component, which dominates more significantly on the dark current performance as reverse bias increases. Therefore, the activation energy decreases towards the value of half bandgap.

Optical response of the device was measured with a tunable laser. Light from the tunable laser source was coupled into the PD by a lensed fiber, and the input polarization is controlled by a polarization controller. Wavelength dependence of the PD responsivity under -1 V at room temperature is shown in Figure 4. Oscillatory features seen in the spectra are due to the Fabry-Perot resonance between the rear and front facets associated with the ~30% reflection at the waveguide facets. The peak responsivity is about 0.26 A/W at 1300 nm under -1 V. The coupling loss between a spherical-lensed fiber and the waveguide facet was estimated to be 3 dB, which is obtained by measuring the same device as a laser diode under forward bias with integrated sphere power meter and fiber coupled power meter respectively

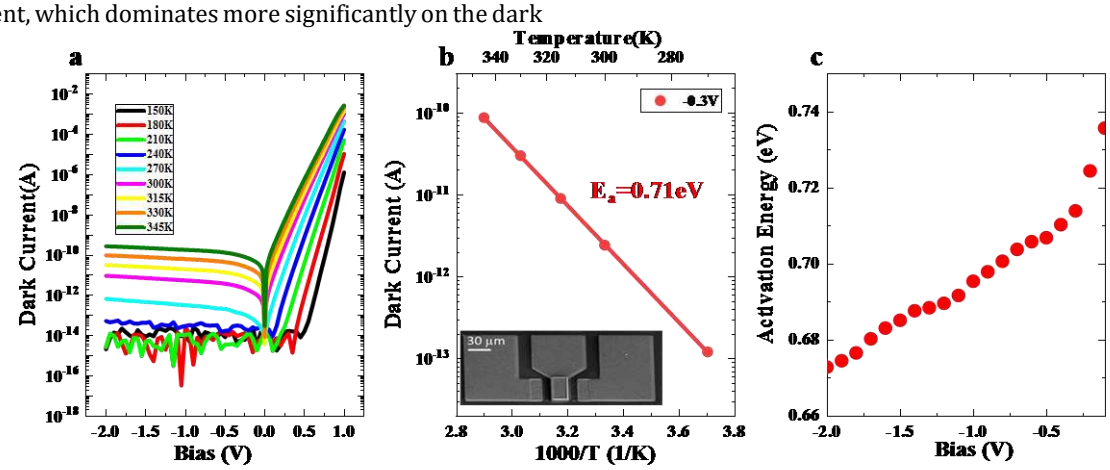

Figure 3. (a) *I-V* characterization of the device as a function of temperature. (b) Arrhenius plot of temperature dependent dark current at -0.3V. Inset: Top-view SEM image of a fabricated device. (c) Dark current activation energy as a function of reverse bias.

After the electrical and optical characterization of the device, LFNS was performed to probe the defect states. The current spectral density of LFNS can be mathematically expressed as [19]:

$$S_I = \sum \frac{A_i \tau_i}{1+(2\pi f \tau_i)^2} + \frac{B}{f} + C \qquad (1)$$

where the three terms represent G-R noise, 1/f noise and white noise, respectively. The G-R noise term appears as Lorentzian peaks in the measured noise spectra, A_i is the amplitudes of the G-R process, τ_i is time constant of each G-R center, B is the amplitudes of the1/f process, and C is a constant related with white noise. In order to make the Lorentzian component more visible from the spectrum, eq (1) is multiplied by f, which is expressed as:

$$fS_I = \sum \frac{fA_i \tau_i}{1+(2\pi f \tau_i)^2} + B + fC \qquad (2)$$

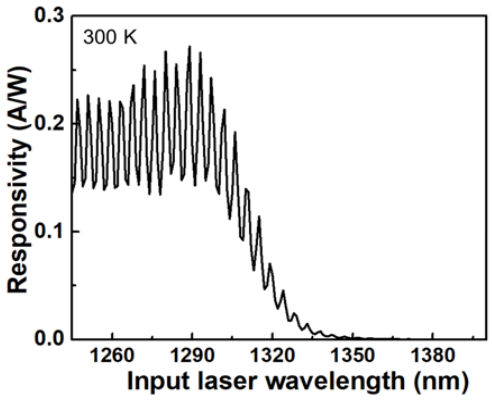

Figure 4. Wavelength dependence of PD responsivity at room temperature biased at -1 V.

In order to probe the physically meaningful trap parameters such as energy and cross section from the measured spectra, the noise spectra at different temperatures and applied bias were measured. By fitting the measured noise spectra with eq (2), the lifetime τ_i under different temperatures can be extracted [20-21]. From an Arrhenius plot of $\ln(\tau T^2)$ versus $1000/T$, the energy level of the trap states can be extracted from the

slope, and the capture cross section can be found from the intercept [22].

The LFNS of the device was measured over a temperature range from 180-430 K with a step of 10 K, under a bias voltage of 300 mV. Figure 5(a) shows the measured noise spectra within the temperature range at which G-R noise was evident. The time constant is extracted by Lorentzian fitting. With these data, the Arrhenius plot $\ln(\tau T^2)$ versus $1000/T$ is shown in Figure 5(b). A defect level with an activation energy of 0.4 eV is extracted with a capture cross section of 1.5×10^{-16}cm^2. Hence, this defect level isnear the middle of bandgap (E_g=0.92 eV). However, trap density (N_t) could not be obtained with LFNS measurement due to the sensitivity of Lorentzian amplitudes to the applied bias conditions. Further analysis of I-V and Capacitance-Voltage (*C-V*) characteristics were used to investigate the trap density. From Arrhenius plot of dark current (Figure 3(b)), it is concluded that the dark current is dominated by both diffusion and G-R components. In this scenario, one can write the dark current under reverse bias as follows:

$$I_R = I_{diff} + I_{gen} \tag{3}$$

Under reverse bias, I_{diff} is saturation current for an ideal diffusion current given by [23]:

$$I_{\text{diff}} = Aqn_{\text{i}}^2\left(\frac{D_n}{L_nN_A}+\frac{D_p}{L_pN_D}\right) \tag{4}$$

where N_A and N_D are the doing of P and N region of the p-i-n structure, A is the device area, q is the electron charge, n_i is intrinsic carrier concentration, L_n (L_p) and D_n (D_p) are the diffusion length and diffusion coefficient for electron (hole) respectively. I_{gen} is G-R current and can be expressed as:

$$I_{\text{gen}} = \frac{Aqn_iW_a}{\tau_g} \tag{5}$$

where W_a is depletion region thickness of the device, τ_g is the generation lifetime. From eq (3)-(5) it is found that generation-recombination current increases linearly with depletion region thickness W_a [24]. Here, the depletion region width can be determined by *C-V* characteristics of the device under 300 K as shown in Figure 6(a), and we calculated the W_a using $W_a = \frac{A\varepsilon}{C_d}$ (where C_d is the capacitance, ε is the static dielectric constant). Thus, by plotting dark current against depletion region thickness one can obtain the generation lifetime from the slope of the linear part. Figure 6(b) shows the dark current density as a function of depletion region thickness, with the bias voltage increasing from -0.04 to -2 V. From the slope of the fitting curve, we obtained τ_g of 2.7×10^{-4} s of the device at 300 K. It is noted that the linear relation between dark current density and W_a maintains well only when the W_a is lower than 0.13 μm (corresponding to a bias below -1.32 V), when the bias goes beyond -1.32 V, the linear characteristics deviates, which may be due to the parasitic capacitance in the contact pad. The parasitic could cause a reduction of calculated W_a in the high bias region, thus, affecting the linear relation between dark current density and W_a. After τ_g is determined, the associated recombination lifetime can be estimated by [25-26]:

$$\tau_{\text{r}} = \tau_g/[2\cosh((E_T-E_i)/k_BT)] \tag{6}$$

where τ_r is the recombination lifetime, k_B is the Boltzmann constant, T is the device temperature, E_T and E_i are the energy level of defect and intrinsic Fermi level, respectively. A recombination lifetime of 27 μs is obtained by eq (6). Finally, a trap density of N_t=5.4×10^{12} cm^{-3} was estimated using the following formula:

$$N_{\text{t}} = 1/(\tau_{\text{n}}\sigma_n v_{\text{th}}) = 1/(\tau_r\sigma_n v_{\text{th}}) \tag{7}$$

where τ_n is recombination lifetime of electron, σ_n is the capture cross section of electron, v_{th} is the thermal velocity. This trap density is comparable to that of the InAs/InGaAs QDs structure grown on native GaAs substrate (in the range of 10^{12} to 10^{14} cm^{-3}) [27-28].

Finally, we want to point out that since the dark current observed in the QD p-i-n photodiodes correlates to native defects in the materials, there is still room to further decrease the dark current with longer carrier lifetime and lower defect density[18, 29]. In addition, the carrier lifetime extracted here can be used to model the carrier dynamics process and quantum efficiency in the QD p-i-n photodiodes. Longer carrier lifetime could also help the photodiodes to sweep the photo-generated carriers out of the absorption region more efficiently, and better quantum efficiency could be expected. Thus, an improving photodiode performance can be achieved by further optimizing the growth condition and reducing defect density. Furthermore, the III-V QDs on Si structure demonstrated in this work could also operate as a laser diode on Si as they share the same epitaxial structure[14], the defect information and the lifetime obtained in this work correlates to the amplitude of non-radiative recombination process, which is critical for laser threshold analysis and laser dynamics modeling to investigate the thermal characteristics, relaxation oscillation parameter and modulation properties [30-31]. It is also noted that using a n-i-n structure, a slight variation of the current p-i-n structure, the current near-infrared photodetector structure can be transferred into quantum dot infrared photodetector (QDIP) structure utilizing inter-subband absorption to detect mid-wavelength infrared light, which has important applications in both civil and military areas [5-6, 32]. The density of deep traps and trap energy levels play an important role with the QD energy levels to model the self-consistent band bending and space charge distribution, which determines the electron occupancy in QDs, a critical parameter in inter-subband QDIP device to further optimize the dark current and responsivity performance[27].

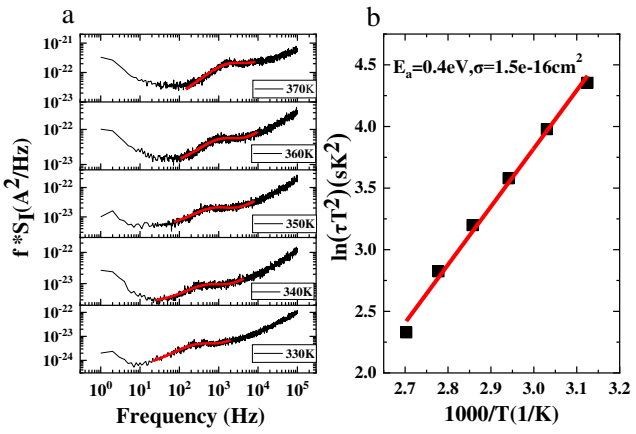

Figure 5. (a) Measured noise spectra under different temperature with Lorentzian fitting. (b) Arrhenius plot for the trap detected by LFNS in the device.

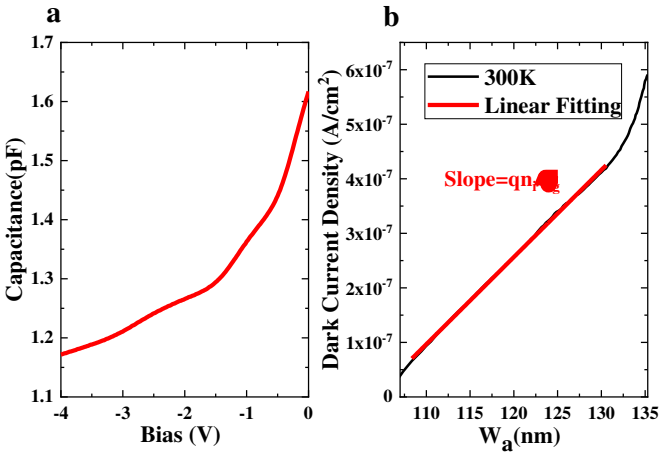

Figure 6. (a)The C-V curve of the device under 300K. (b) Dark current density versus depletion region thickness at 300 K of the device.

CONCLUSIONS

In conclusion, III-V QD PD on Si with lowest dark current density among all III-V on Si PDs was demonstrated, to our best knowledge, and low frequency noise spectroscopy was carried out to study quantitatively the defect information in the III-V QD PD structure monolithically grown on Si. One trap level with activation energy of 0.4 eV was identified along with a capture cross section of 1.5×10^{-16}cm^2. Based on a simple electrical method, the trap density of 5.4×10^{12} cm^{-3} can be extracted. The defect information found in the photodiode may help further optimize the material growth and pave the way towards monolithic photonic integrated circuits directly grown on CMOS compatible Si substrates.

AUTHOR INFORMATION

Corresponding Author

* E-mail: chenbl@shanghaitech.edu.cn. (Baile Chen)

Author Contributions

‡These authors contributed equally to this work.

Notes

The authors declare no competing financial interest.

ACKNOWLEDGMENTS

This study is supported by Shanghai Sailing Program (17YF1429300), ShanghaiTech University startup funding (F-0203-16-002) and Advanced Research Projects Agency-Energy (ARPA-E) DE-AR000067.

REFERENCES

1. Krishna, S., Quantum dots-in-a-well infrared photodetectors. *J. Phys. D: Appl. Phys.* **2005,** *38* (13), 2142-2150.
2. Chakrabarti, S.; Stiff-Roberts, A. D.; Bhattacharya, P.; Gunapala, S.; Bandara, S.; Rafol, S. B.; Kennerly, S. W., High-Temperature Operation of InAs–GaAs Quantum-Dot Infrared Photodetectors With Large Responsivity and Detectivity. *IEEE Photonics Technol. Lett.* **2004,** *16* (5), 1361-1363.
3. Chen, S.; Li, W.; Wu, J.; Jiang, Q.; Tang, M.; Shutts, S.; Elliott, S. N.; Sobiesierski, A.; Seeds, A. J.; Ross, I.; Smowton, P. M.; Liu, H., Electrically pumped continuous-wave III–V quantum dot lasers on silicon. *Nat. Photonics* **2016,** *10* (5), 307-311.
4. Tang, M.; Chen, S.; Wu, J.; Jiang, Q.; Dorogan, V. G.; Benamara, M.; Mazur, Y. I.; Salamo, G. J.; Seeds, A.; Liu, H., 1.3-mum InAs/GaAs quantum-dot lasers monolithically grown on Si substrates using InAlAs/GaAs dislocation filter layers. *Opt Express* **2014,** *22* (10), 11528-35.
5. Chen, W.; Deng, Z.; Guo, D.; Chen, Y.; Mazur, Y. I.; Maidaniuk, Y.; Benamara, M.; Salamo, G. J.; Liu, H.; Wu, J.; Chen, B., Demonstration of InAs/InGaAs/GaAs Quantum Dots-in-a-Well Mid-Wave Infrared Photodetectors Grown on Silicon Substrate. *Journal of Lightwave Technology* **2018,** *36* (13), 2572-2581.
6. Huang, J.; Guo, D.; Deng, Z.; Chen, W.; Liu, H.; Wu, J.; Chen, B., Midwave Infrared Quantum Dot Quantum Cascade Photodetector Monolithically Grown on Silicon Substrate. *Journal of Lightwave Technology* **2018,** *36* (18), 4033-4038.
7. Li, Q.; Ng, K. W.; Lau, K. M., Growing antiphase-domain-free GaAs thin films out of highly ordered planar nanowire arrays on exact (001) silicon. *Appl. Phys. Lett.* **2015,** *106* (7).
8. Liu, A. Y.; Herrick, R. W.; Ueda, O.; Petroff, P. M.; Gossard, A. C.; Bowers, J. E., Reliability of InAs/GaAs Quantum Dot Lasers Epitaxially Grown on Silicon. *IEEE Journal of Selected Topics in Quantum Electronics* **2015,** *21* (6), 690-697.
9. Petroff, P.; Hartman, R. L., Defect structure introduced during operation of heterojunction GaAs lasers. *Appl. Phys. Lett.* **1973,** *23* (8), 469-471.
10. Kimerling, L., Recombination enhanced defect reactions. *Solid State Electron.* **1978,** *21* (11-12), 1391-1401.
11. Jung, D.; Herrick, R.; Norman, J.; Turnlund, K.; Jan, C.; Feng, K.; Gossard, A. C.; Bowers, J. E., Impact of threading dislocation density on the lifetime of InAs quantum dot lasers on Si. *Appl. Phys. Lett.* **2018,** *112* (15), 153507.
12. Li, W.; Chen, S.; Tang, M.; Wu, J.; Hogg, R.; Seeds, A.; Liu, H.; Ross, I., Effect of rapid thermal annealing on threading dislocation density in III-V epilayers monolithically grown on silicon. *Journal of Applied Physics* **2018,** *123* (21), 215303.
13. Li, Q.; Wan, Y.; Liu, A. Y.; Gossard, A. C.; Bowers, J. E.; Hu, E. L.; Lau, K. M., 1.3-mum InAs quantum-dot micro-disk lasers on V-groove patterned and unpatterned (001) silicon. *Opt Express* **2016,** *24* (18), 21038-45.
14. Wan, Y.; Norman, J.; Li, Q.; Kennedy, M.; Liang, D.; Zhang, C.; Huang, D.; Zhang, Z.; Liu, A. Y.; Torres, A., 1.3 μm submilliamp threshold quantum dot micro-lasers on Si. *Optica* **2017,** *4* (8), 940-944.
15. Wan, Y.; Zhang, Z.; Chao, R.; Norman, J.; Jung, D.; Shang, C.; Li, Q.; Kennedy, M. J.; Liang, D.; Zhang, C.; Shi, J. W.; Gossard, A. C.; Lau, K. M.; Bowers, J. E., Monolithically integrated InAs/InGaAs quantum

dot photodetectors on silicon substrates. *Opt Express* **2017,** *25* (22), 27715-27723.
16. Wan, Y.; Li, Q.; Geng, Y.; Shi, B.; Lau, K. M., InAs/GaAs quantum dots on GaAs-on-V-grooved-Si substrate with high optical quality in the 1.3 μ m band. *Appl. Phys. Lett.* **2015,** *107* (8), 081106.
17. Inoue, D.; Wan, Y.; Jung, D.; Norman, J.; Shang, C.; Nishiyama, N.; Arai, S.; Gossard, A.; Bowers, J., Low-dark current 10 Gbit/s operation of InAs/InGaAs quantum dot pin photodiode grown on on-axis (001) GaP/Si. *Applied Physics Letters* **2018,** *113* (9), 093506.
18. Chen, H.; Verheyen, P.; De Heyn, P.; Lepage, G.; De Coster, J.; Balakrishnan, S.; Absil, P.; Roelkens, G.; Van Campenhout, J., Dark current analysis in high-speed germanium pin waveguide photodetectors. *Journal of Applied Physics* **2016,** *119* (21), 213105.
19. Jones, B. K., Low-frequency noise spectroscopy. *IEEE Trans. Electron Devices* **1994,** *41* (11), 2188-2197.
20. Chen, W.; Chen, B.; Holmes, A.; Fay, P., Investigation of traps in strained-well InGaAs/GaAsSb quantum well photodiodes. *Electron. Lett.* **2015,** *51* (18), 1439-1440.
21. Chen, W.; Chen, B.; Yuan, J.; Holmes, A.; Fay, P., Bulk and interfacial deep levels observed in In0. 53Ga0. 47As/GaAs0. 5Sb0. 5 multiple quantum well photodiode. *Appl. Phys. Lett.* **2012,** *101* (5), 052107.
22. Schroder, D. K., *Semiconductor material and device characterization*. John Wiley & Sons: 2006; p 262.
23. Sze, S. M.; Ng, K. K., *Physics of semiconductor devices*. John wiley & sons: 2006; p 94.
24. Simoen, E.; Claeys, C.; Vanhellemont, J., Defect Analysis in Semiconductor Materials Based on p-n Junction Diode Characteristics. *Defect and Diffusion Forum* **2007,** *261-262*, 1-24.
25. Schroder, D., The concept of generation and recombination lifetimes in semiconductors. *IEEE Trans. Electron Devices* **1982,** *29* (8), 1336-1338.
26. Simoen, E.; Claeys, C., On the impact of the capture rates on the generation/recombination lifetime ratio of a single deep level. *IEEE Trans. Electron Devices* **1999,** *46* (7), 1487-1488.
27. Asano, T.; Fang, Z.; Madhukar, A., Deep levels in GaAs (001)/InAs/InGaAs/GaAs self-assembled quantum dot structures and their effect on quantum dot devices. *Journal of Applied Physics* **2010,** *107* (7), 073111.
28. Kunets, V. P.; Morgan, T. A.; Mazur, Y. I.; Dorogan, V.; Lytvyn, P.; Ware, M.; Guzun, D.; Shultz, J.; Salamo, G., Deep traps in GaAs/InGaAs quantum wells and quantum dots, studied by noise spectroscopy. *J. Appl. Phys.* **2008,** *104* (10), 103709.
29. Chen, B.; Yuan, J.; Holmes, A., Dark current modeling of InP based SWIR and MWIR InGaAs/GaAsSb type-II MQW photodiodes. *Optical and Quantum Electronics* **2012**, 1-7.
30. Lingnau, B.; Lüdge, K.; Chow, W. W.; Schöll, E., Influencing modulation properties of quantum-dot semiconductor lasers by carrier lifetime engineering. *Applied Physics Letters* **2012,** *101* (13), 131107.
31. Fitch, C. R.; Marko, I.; Baltusis, A.; Adams, A.; Jung, D.; Norman, J. C.; Bowers, J. E.; Sweeney, S. J. In *Thermal characteristics of 1.3 um InAs-based quantum-dot lasers on silicon substrates (Conference Presentation)*, Novel In-Plane Semiconductor Lasers XVIII, International Society for Optics and Photonics: 2019; p 109390Q.
32. Wu, J.; Jiang, Q.; Chen, S.; Tang, M.; Mazur, Y. I.; Maidaniuk, Y.; Benamara, M.; Semtsiv, M. P.; Masselink, W. T.; Sablon, K. A., Monolithically integrated InAs/GaAs quantum dot mid-infrared photodetectors on silicon substrates. *ACS Photonics* **2016,** *3* (5), 749-753.